Calculating locally conservative velocity fields using discontinuous enrichment and other non-conforming finite elements

brown-bag lunch seminar

M.W. Farthing[1] C.E. Kees[1]

[1]U.S. Army Engineer Research and Development Center

February 27 2008

Context: Numerical Methods for Subsurface Flow and Transport

- There are increasing demands on simulators to handle larger, more complex problems
- Unstructured meshes are often desirable because of domain geometry and/or local adaption strategies
- Locally conservative velocity fields are desirable when simulating coupled flow and transport
- ADH is intended for simulating large scale coupled flow and transport problems on locally adapted, unstructured meshes (in parallel)

Locally Conservative Methods

Local conservation has long been a motivating factor in method development (FVM, MFEM, MPFA, CV-MFEM, ...)

$$\mathcal{E}(n) = \{8, 9, 17, 18, 19\}$$
$$e^* = \{1, 5, 2, 3, 4\}$$

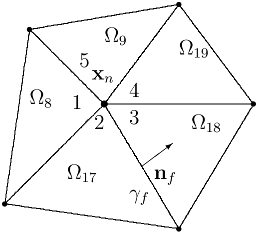

$$e_\ell(f) = 17,\ e_r(f) = 18$$
$$e_\ell^*(f) = 2,\ e_r^*(f) = 3$$

Element-based conservation

$$\int_{\Omega_e} (\hat{m}_t - b)\, \mathrm{d}x + \int_{\partial\Omega_e} \boldsymbol{\sigma}_h \cdot \mathbf{n}\, \mathrm{d}s = 0$$

Locally Conservative Methods

- Traditional postprocessing techniques for conforming Galerkin (CG) FEMs were often of limited applicability, unwieldy, or just ignored
- ADH is built on stabilized, conforming FEM approximations

Goals

1. Summarize a multiscale stabilized FEM for Richards' equation
2. Combine this with postprocessing algorithms for subsurface velocity fields
3. Evaluate the combined approaches' performance and compare them with a locally conservative nonconforming FEM.

Outline

Variably Saturated Groundwater Flow

$$
\begin{aligned}
m_t + \nabla \cdot (\rho \mathbf{q}) &= b, \text{ for } \mathbf{x}, t \in \Omega \times [0, T] && (1)\\
m &= \rho\theta && (2)\\
\mathbf{q} &= -k_r \boldsymbol{K}_s \left(\nabla\psi - \rho \mathbf{g}_u\right) && (3)
\end{aligned}
$$

with

$$
\psi = \psi^b, \text{ on } \Gamma_D, \quad \rho\mathbf{q}\cdot\mathbf{n} = q^b, \text{ on } \Gamma_N \qquad (4)
$$

$$
\rho = \rho(\psi), \theta = \theta(\psi, \mathbf{x}), k_r = k_r(\psi, \mathbf{x})
$$

Nonlinear, Scalar PDE

Rewrite as generic nonlinear advection-diffusion equation for convenience ...

$$
\begin{aligned}
m_t + \nabla \cdot (\mathbf{f} - \boldsymbol{a}\nabla\psi) &= b && (5)\\
\mathbf{f} &= \rho^2 k_r \boldsymbol{K}_s \mathbf{g}_u, && (6)\\
\boldsymbol{a} &= \rho k_r \boldsymbol{K}_s && (7)\\
\boldsymbol{\sigma} &= \mathbf{f} - \boldsymbol{a}\nabla\psi && (8)
\end{aligned}
$$

where $\boldsymbol{\sigma} = \rho\mathbf{q}$

Multiscale Finite Element Discretization

Strong form of Dirichlet problem: find $u : \Omega \to \mathbb{R}$ such that

$$\begin{aligned} \mathcal{R} &:= m_t + \nabla \cdot [\mathbf{f} - \boldsymbol{a}\nabla\psi] - b = 0 \\ & \quad \forall x \in \Omega \end{aligned} \tag{9}$$

$$\begin{aligned} \psi &= \psi^b(x), \quad \text{for } x \in \Gamma_D \\ \boldsymbol{\sigma} \cdot \mathbf{n} &= \sigma^b, \quad \text{for } x \in \Gamma_N \end{aligned} \tag{10}$$

Discretize m_t first (Rothe's method) using a standard BDF approximation

$$m_t \approx \hat{m}_t = \alpha^{n+1} m + \beta^n \tag{11}$$

Multiscale Finite Element Discretization (cont'd)

Multiscale weak form: find $\psi \in V = V_h \oplus \delta V$ such that

$$
\begin{aligned}
F_h &= \int_\Omega \hat{m}_t w_h \, \mathrm{d}x - \int_\Omega (\mathbf{f} - \boldsymbol{a}\nabla\psi) \cdot \nabla w_h \, \mathrm{d}x - \int_\Omega b w_h \, \mathrm{d}x \\
&= -\int_{\Gamma_N} \sigma^b w_h \, \mathrm{d}s \quad \forall w_h \in W_h && (12) \\
F_\delta &= \int_\Omega \hat{m}_t \delta w \, \mathrm{d}x - \int_\Omega (\mathbf{f} - \boldsymbol{a}\nabla\psi) \cdot \nabla \delta w \, \mathrm{d}x - \int_\Omega b \delta w \, \mathrm{d}x \\
&= -\int_{\Gamma_N} \sigma^b \delta w \, \mathrm{d}s \quad \forall \delta w \in \delta W && (13)
\end{aligned}
$$

Hughes(1995), Juanes and Patzek(2005)

Multiscale Finite Element Discretization (cont'd)

The goal is to obtain a modified version of eqn (12)

$$G_h = F_h - \sum_e \int_{\Omega_e} \mathcal{L}^*_{s,h} w_h \tau \mathcal{R}_h(\psi_h)\,\mathrm{d}x = 0, \forall w_h \in W_h \quad (14)$$

and a corresponding linearized system of equations to use in a Newton solution algorithm for ψ_h.
Here, $\mathcal{R}_h$ is an approximation to $\mathcal{R}$ from eqn (9) and and $\mathcal{L}^*_{s,h}$ approximates the formal adjoint of a linear operator $\mathcal{L}_s$ defined in the linearization process.

Multiscale Newton Iteration

Given a current iterate, ψ_h^-, we label the Newton increment $v = v_h + \delta v$ and linearize around ψ_h^-

$$\int_\Omega \hat{m}_t' v w_h \,\mathrm{d}x - \int_\Omega \left(\mathbf{f}' v - \boldsymbol{a}' \nabla \psi_h^- v - \boldsymbol{a} \nabla v\right) \cdot \nabla w_h \,\mathrm{d}x = -F_h^- \quad \forall w_h \in W_h \tag{15}$$

$$\int_\Omega \hat{m}_t' v \delta w \,\mathrm{d}x - \int_\Omega \left(\mathbf{f}' v - \boldsymbol{a}' \nabla \psi_h^- v - \boldsymbol{a} \nabla v\right) \cdot \nabla \delta w \,\mathrm{d}x = -F_\delta^- \quad \forall \delta w \in \delta W \tag{16}$$

Here, the $'$ symbol represents differentiation with respect to ψ.

Subgrid-scale equation

Assume $\delta w = \delta v = 0$ on $\partial\Omega_e$ to localize eqn (16). Do some manipulations to come up with

$$\int_{\Omega_e} \mathcal{L}\delta v \delta w \,\mathrm{d}x = -\int_{\Omega_e} \mathcal{L}v_h \delta w \,\mathrm{d}x - \int_{\Omega_e} \mathcal{R}(\psi_h^-)\delta w \,\mathrm{d}x \quad (17)$$

where

$$\begin{aligned} \mathcal{L}v &= \hat{m}_t' v + \nabla \cdot \left[\mathbf{f}' v - \boldsymbol{a}'\nabla\psi_h^- v - \boldsymbol{a}\nabla v\right] \\ &= \hat{m}_t' v + \mathcal{L}_s v \end{aligned} \quad (18)$$

$\mathcal{L}v_h$ can be understood as a grid-scale linearization of $\mathcal{R}(\psi_h^-)$ on each Ω_e.

Grid-scale equation

Collect terms in eqn (15), integrate by parts, neglect temporal variation in subgrid scales to get

$$\int_{\Omega} \hat{m}'_t v_h w_h \,\mathrm{d}x - \int_{\Omega} \left(\mathbf{f}' v_h - \boldsymbol{a}' \nabla \psi_h v_h - \boldsymbol{a} \nabla v_h\right) \cdot \nabla w_h \,\mathrm{d}x + \sum_e \int_{\Omega_e} \mathcal{L}_s^* w_h \delta v \,\mathrm{d}x = -F_h^- \quad (19)$$

Here, the formal adjoint of $\mathcal{L}_s$ has been introduced

$$\mathcal{L}_s^* w = -\left(\mathbf{f}' - \boldsymbol{a}' \nabla \psi_h^-\right) \cdot \nabla w - \nabla \cdot (\boldsymbol{a} \nabla w) \quad (20)$$

More Approximations

ASGS assumption

$$\delta v \approx -\tau\left(\mathcal{L}_h v_h + \mathcal{R}_h^-\right) \tag{21}$$

$$\tau = \left[\left(2\frac{\|\mathbf{f}' - \boldsymbol{a}'\nabla\psi_h\|_2}{h_e}\right)^2 + 9\left(4\frac{\|\boldsymbol{a}\|_\infty}{h_e^2}\right)^2\right]^{-\frac{1}{2}} \tag{22}$$

Isotropic shock-capturing ...

$$\begin{aligned} G_h &= F_h - \sum_e \int_{\Omega_e} \mathcal{L}^*_{s,h} w_h \tau \mathcal{R}_h(\psi_h)\,\mathrm{d}x + \sum_e \int_{\Omega_e} \nu \nabla\psi_h \cdot \nabla w_h \,\mathrm{d}x \\ &= 0, \forall w_h \in W_h \end{aligned} \tag{23}$$

Element-based local mass conservation

We would like an approximate $\boldsymbol{\sigma}_h$ that

- conserves mass discretely on each element, Ω_e

$$\int_{\Omega_e} (\hat{m}_t - b)\,\mathrm{d}x + \int_{\partial\Omega_e} \boldsymbol{\sigma}_h \cdot \mathbf{n}\,\mathrm{d}s = 0 \tag{24}$$

- has continuous normal component across (interior) faces, γ_f
- is cheap/simple to compute

Larson and Niklasson (2004) Postprocessing

Start with a uniquely defined velocity on element faces, $\bar{\boldsymbol{\sigma}}_{h,f}$

- Define piecewise contant correction at each face (see Fig. 18)

$$\hat{\boldsymbol{\sigma}}_{h,f} = \bar{\boldsymbol{\sigma}}_{h,f} + \frac{1}{|\gamma_f|}\left(U_{e_\ell(f)} - U_{e_r(f)}\right)\mathbf{n}_f \tag{25}$$

- insert $\hat{\boldsymbol{\sigma}}_{h,f}$ into mass conservation statement, eqn (24), and obtain $N_e \times N_e$ system for the element corrections $\{U_e\}$

Mesh Notation

$$\mathcal{E}(n) = \{8, 9, 17, 18, 19\}$$
$$e^* = \{1, 5, 2, 3, 4\}$$

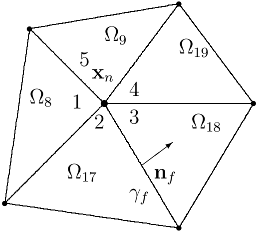

$$e_\ell(f) = 17,\ e_r(f) = 18$$
$$e^*_\ell(f) = 2,\ e^*_r(f) = 3$$

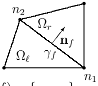

$\mathcal{N}(f) = \{n_1, n_2\}$

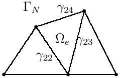

$\mathcal{F}_{i,d}(e) = \{22, 23\}$

Implementation

Since using C^0P^1 approximation, associate test function $w_{h,n}$ with nodes $\mathbf{x}_n$, $n = 1, \ldots, N_n$ define discrete residual associated with each $e \in \mathcal{E}(n)$ as

$$
\begin{aligned}
G_{h,n,e} &= \int_{\Omega_e} \hat{m}_t w_{h,n}\, \mathrm{d}x - \int_{\Omega_e} \left(\mathbf{f} - \boldsymbol{a}\nabla\psi_h\right) \cdot \nabla w_{h,n}\, \mathrm{d}x \\
&\quad - \int_{\Omega_e} b w_{h,n}\, \mathrm{d}x - \int_{\Omega_e} \mathcal{L}^*_{s,h} w_{h,n} \tau \mathcal{R}_h(\psi_h)\, \mathrm{d}x \\
&\quad + \int_{\Omega_e} \nu \nabla\psi_h \cdot \nabla w_{h,n}\, \mathrm{d}x + \int_{\partial\Omega_e \cap \Gamma_N} \sigma^b w_{h,n}\, \mathrm{d}s \qquad (26)
\end{aligned}
$$

and element residual

$$
G_{h,e} = \sum_{n \in \mathcal{N}(e)} G_{h,n,e} \qquad (27)
$$

VPP (cont'd)

$\hat{\boldsymbol{\sigma}}_h$ at each face is defined to be the average plus a piecewise linear correction

$$\hat{\boldsymbol{\sigma}}_{h,f} = \bar{\boldsymbol{\sigma}}_{h,f} + \sum_{n \in \mathcal{N}(f)} \left(U_{n,e^*_\ell(f)} - U_{n,e^*_r(f)} \right) \mathbf{n}_f w_{h,n} \qquad (28)$$

where $w_{h,n}$ is the piecewise linear test function associated with $\mathbf{x}_n$. The corrections, $U_{n,e}$ are determined by requiring

$$\begin{aligned} R_{n,e^*} &= G_{h,n,e} \qquad (29) \\ &+ \sum_{f \in \mathcal{F}_{i,d}(e)} \int_{\gamma_f} \left[\bar{\boldsymbol{\sigma}}_{h,f} + \left(U_{n,e^*_\ell(f)} - U_{n,e^*_r(f)} \right) \mathbf{n}_f \right] w_{h,n} \cdot \mathbf{n}_e \, \mathrm{d}s \end{aligned}$$

for all $\mathbf{x}_n$ and $\Omega_e \in \mathcal{E}(n)$

VPP (cont'd)

- Element conservation follows directly from eqn (30) and fact that test functions are a partition of unity.
- After solving for corrections on each face, we extend velocity field to whole domain by either projecting onto RT0

$$\hat{\mathbf{V}}_h(\Omega_e) = [P^0(\Omega_e)]^{n_d} \oplus \mathbf{x}P^0(\Omega_e) \tag{30}$$

- RT0 discards some information from $\hat{\boldsymbol{\sigma}}_h$, but it is very cheap and we only expect first order accuracy anyway, Larson and Niklasson(2004).

Sun-Wheeler Postprocessing

Sun and Wheeler(2006) presents both global and local postprocessing algorithms for $\hat{\boldsymbol{\sigma}}_h$ from a minimization perspective.

$$R_e = \sum_{n \in \mathcal{N}(e)} G_{h,n,e} + \sum_{\gamma_f \in \partial\Omega_e} \int_{\gamma_f} \left(\bar{\boldsymbol{\sigma}}_{h,f} + \Delta U_f \mathbf{n}_f \right) \cdot \mathbf{n}_e \, \mathrm{d}s, \quad e = 1, \ldots, N_e \tag{31}$$

Local version computes corrections on each γ_f based on minimizing

$$\left[\int_\Omega \bar{R}^2 \, \mathrm{d}x \right]^{1/2} \tag{32}$$

where $\bar{R}|_{\Omega_e} = \bar{R}_e = R_e / |\Omega_e|$

P^1 nonconforming approximation

For comparison, we consider a simple P^1 nonconforming approximation, find $\psi_h \in V_h^{nc}$

$$\int_\Omega \hat{m}_t w_h \, \mathrm{d}x - \int_\Omega (\mathbf{f} - \boldsymbol{a}\nabla\psi_h) \cdot \nabla w_h \, \mathrm{d}x + \int_{\Gamma_N} \sigma^b w_h \, \mathrm{d}s - \int_\Omega b w_h \, \mathrm{d}x = 0 \forall w_h \in W_h^{nc} \tag{33}$$

with trial space

$$V_h^{nc} = \{v : v|_{\Omega_e} \in P^1(\Omega_e), \ \forall \Omega_e \in T_h; v \text{ cont. at } \bar{\mathbf{x}}_f, \ \forall \gamma_f \in \Gamma_I; \ v = \psi^b \text{ at } \bar{\mathbf{x}}_f, \ \forall \gamma_f \in \Gamma_D\} \tag{34}$$

P^1 NC shape functions

Locally use the Crouzeix-Raviart space with basis

$$\begin{aligned} N_i &= n_d\left(\frac{1}{n_d} - \lambda_i\right), \\ \lambda_i &= 1 - \frac{(\mathbf{x}-\mathbf{x}_i)\cdot\mathbf{n}_i}{(\mathbf{x}_{i+1}-\mathbf{x}_i)\cdot\mathbf{n}_i} \\ \nabla N_i &= |\gamma_i|\mathbf{n}_i/|\Omega_e| \end{aligned}$$

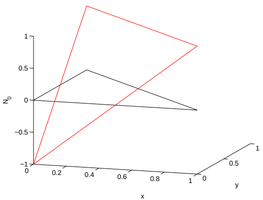

$i = 1, \ldots, n_d + 1$

P^1 NC velocity

Define local velocity approximation

$$\hat{\boldsymbol{\sigma}}_{h,e} = \bar{\mathbf{f}}_e - \bar{\boldsymbol{a}}_e \nabla \psi_h + \frac{\bar{d}_e}{n_d}(\mathbf{x} - \bar{\mathbf{x}}_e) + \mathbf{c}_e \tag{35}$$

where $\bar{\boldsymbol{a}}_e$ and $\bar{\mathbf{f}}_e$ represent averages (componentwise) over Ω_e

$$\bar{d}_e = \frac{1}{|\Omega_e|}\int_{\Omega_e} (b - \hat{m}_t)\, \mathrm{d}x = \bar{b}_e - \bar{\hat{m}}_{t,e} \tag{36}$$

$\boldsymbol{\sigma}_{h,e}$ is in the lowest order Raviart-Thomas space on Ω_e, (see 30). Local conservation

$$\begin{aligned}\int_{\Omega_e} \hat{m}_t \,\mathrm{d}x + \int_{\Omega_e} \nabla \cdot \hat{\boldsymbol{\sigma}}_{h,e}\,\mathrm{d}x - \int_{\Omega_e} b\,\mathrm{d}x &= |\Omega_e|\left(\bar{\hat{m}}_{t,e} - \bar{b}_e\right) + \bar{d}_e|\Omega_e| \\ &= 0\end{aligned}$$

P^1 NC velocity (cont'd.)

The piecewise constant $\mathbf{c}_e$ serves to enforce continuity at element interfaces and requires, in general, the solution of a local $n_d \times n_d$ system on each element, Chou and Tang(2000)

$$\begin{aligned} \boldsymbol{B}_e^{nc}\mathbf{c}_e &= \boldsymbol{\eta}_e \\ B_{e,ij} &= |\partial\Omega_{e,i}| n^j_{e,i}, \; i,j = 1,\dots,n_d \\ \eta_{e,i} &= \int_{\Omega_e} b w_{h,i}\,\mathrm{d}x - \frac{|\Omega_e|}{n_d+1}\bar{b}_e - \int_{\Omega_e} \hat{m}_t w_{h,i}\,\mathrm{d}x + \frac{|\Omega_e|}{n_d+1}\bar{\hat{m}}_t \end{aligned} \tag{37}$$

P^1 NC (cont'd)

eqn (33) and eqn (35) (with $\mathbf{c}_e = 0$) yield solutions equivalent to a MHFEM discretization with the correct L_2 projections and assumptions on the problem data, Marini(1985), Arbogast and Chen(1995), Chen(1996). Find $(\psi_h, \boldsymbol{\sigma}_h, \Lambda_h)$ in $(W_h, \mathbf{W}_h, L_h)$ such that

$$
\begin{aligned}
\int_\Omega \hat{m}_t w_h \,\mathrm{d}x + \int_\Omega \nabla \cdot \boldsymbol{\sigma}_h w_h \,\mathrm{d}x &= \int_\Omega b w_h \,\mathrm{d}x, \ \forall w_h \in W_h \\
\int_\Omega \mathbf{a}^{-1}(\boldsymbol{\sigma}_h - \mathbf{f}) \cdot \mathbf{w}_h + \int_\Omega \Lambda_h \mathbf{w}_h \cdot \mathbf{n} \,\mathrm{d}s &= \int_\Omega \psi_h \nabla \cdot \mathbf{w}_h \,\mathrm{d}x, \ \forall \mathbf{w}_h \in \mathbf{W}_h \\
\sum_e \int_{\partial\Omega_e} \boldsymbol{\sigma}_h \cdot \mathbf{n}_e \mu_h \,\mathrm{d}s &= 0, \ \forall \mu_h \in L_h,
\end{aligned}
$$

- Can also view $(\psi_h, \hat{\boldsymbol{\sigma}}_h)$ as the solution to a finite volume "box scheme."
- In general, we would like to keep a consistent mass integral because it's less distributed in this case
- If a consistent mass integral is used or source term, we can still recover a locally conservative $\boldsymbol{\sigma}_h$ by solving appropriate element problems for $\mathbf{c}_e = 0$.

Comparisons

We perform a series of numerical experiments to evaluate the accuracy of the CG VPP algorithm and the effectiveness of multiscale stabilization in controlling over/undershoot.

Abbrev.	Definition
CG	conforming Galerkin approximation, eqn (23) with $\tau = 0$, $\nu_c = 0$
CG-S	multiscale stabilized CG with shockcapturing, eqn (23), $\nu_c = 0.1^{\dagger}$
CG-V	lumped CG approximation with vertex quadrature, $\tau = 0$, $\nu_c = 0$
NC	P^1 nonconforming approach

$\dagger$ $\nu_c = 0.5$ for Problem V.

Linear, elliptic problems

Smooth analytical solutions and domain properties

$$\begin{aligned} u(\mathbf{x}) &= \sin^2(2\pi x_1) + \cos^2(2\pi x_2) + x_1 + x_2 + 5 \\ a_{ij}(\mathbf{x}) &= (5 + x_i^2)\delta_{ij} \end{aligned} \tag{38}$$

for $n_d = 2$ and

$$u(\mathbf{x}) = \sum_{i=1}^{3} x_i^2$$

$$a_{ij}(\mathbf{x}) = (5 + x_i^2 x_{i+1})\delta_{ij} \tag{39}$$

for $n_d = 3$.

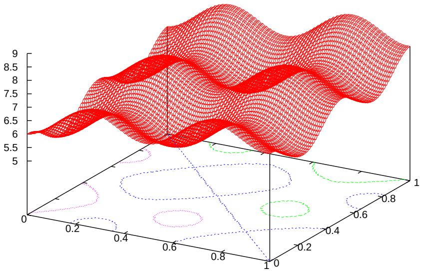

Spatial Error

Table: $\varepsilon_{u,2}$, Problem I

	level	h	N_{dof}	$\varepsilon_{u,2}$	rate
CG	4	0.0442	1089	9.36×10^{-4}	1.98
NC	4	0.0442	3136	9.86×10^{-4}	1.98
CG	5	0.0221	4225	2.35×10^{-4}	1.99
NC	5	0.0221	12416	2.48×10^{-4}	1.99

Table: $\varepsilon_{\sigma,2}$ and ε_{mc}, Problem I

	level	$\varepsilon_{\sigma,2}$	rate	ε_{mc}
CG-PE	4	0.111	0.989	0.628
CG-LN	4	0.110	0.984	0
CG-SW	4	0.111	1.00	0
NC	4	0.110	0.980	0
CG-PE	5	0.0554	0.997	0.205
CG-LN	5	0.0553	0.996	0
CG-SW	5	0.0554	1.00	10^{-6}
NC	5	0.0553	0.994	0

Boundary layer example

Van Genuchten Mualem *p*-*s*-*k* relations, $n_{vg} = 4.264$, $\alpha_{vg} = 5.47$ [1/m], $K_s = 5.04\boldsymbol{I}$ [m/d].

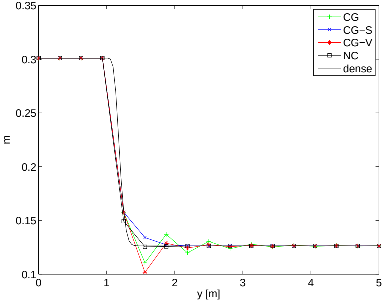

Table: CPU overhead

Method	Level	Its.	CPU [s]
LN	4	-	1.35×10^{-3}
CG-V-SW	4	250	3.33×10^{-2}
CG-S-SW	4	595	6.67×10^{-2}
LN	5	-	5.52×10^{-3}
CG-V-SW	5	83	3.33×10^{-2}
CG-S-SW	5	207	1.17×10^{-1}

Spatial Error

Method	Level†	N_{dof}	$\varepsilon_{\psi,\infty}$	ε_{mc}	$\varepsilon_{\sigma_1,\infty}$	$\varepsilon_{\sigma_2,\infty}$
CG-PE	4	289	8.72×10^{-2}	2.26×10^{-3}	4.40×10^{-3}	2.19×10^{0}
CG-LN	4	289	8.72×10^{-2}	1.35×10^{-8}	4.37×10^{-4}	1.89×10^{-1}
CG-S-LN	4	289	4.36×10^{-2}	3.00×10^{-7}	3.90×10^{-4}	3.65×10^{-1}
CG-S-SW	4	289	4.36×10^{-2}	9.97×10^{-7}	2.10×10^{-3}	6.91×10^{-1}
CG-V-LN	4	289	1.75×10^{-1}	9.33×10^{-9}	2.29×10^{-4}	9.84×10^{-2}
CG-V-SW	4	289	1.75×10^{-1}	9.93×10^{-7}	6.99×10^{-4}	2.49×10^{-1}
NC	4	800	9.49×10^{-2}	0	5.21×10^{-8}	1.66×10^{-4}
CG-PE	5	1089	3.28×10^{-2}	7.17×10^{-4}	2.22×10^{-3}	1.61×10^{0}
CG-LN	5	1089	3.28×10^{-2}	6.10×10^{-8}	3.29×10^{-4}	1.71×10^{-1}
CG-S-LN	5	1089	2.30×10^{-2}	8.88×10^{-8}	3.39×10^{-4}	3.58×10^{-1}
CG-S-SW	5	1089	2.30×10^{-2}	9.97×10^{-7}	1.11×10^{-3}	3.98×10^{-1}
CG-V-LN	5	1089	5.58×10^{-2}	4.92×10^{-9}	2.54×10^{-4}	1.12×10^{-1}
CG-V-SW	5	1089	5.58×10^{-2}	9.98×10^{-7}	4.99×10^{-4}	1.45×10^{-1}
NC	5	3136	2.32×10^{-2}	0	2.71×10^{-7}	1.55×10^{-5}

† $h = 0.319$ on level 4, and $h = 0.160$ on level 5

Block heterogeneous example

Constant recharge into two-dimensional domain, n_{vg} ranges from 1.632 to 5.

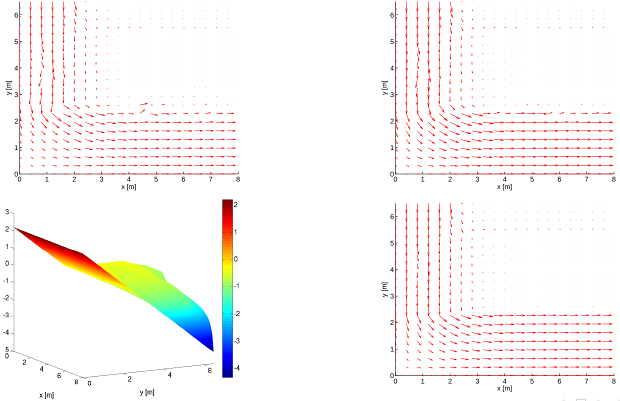

Block heterogeneous example (transient)

Infiltration into two-dimensional domain, n_{vg} ranges from 1.632 to 5.

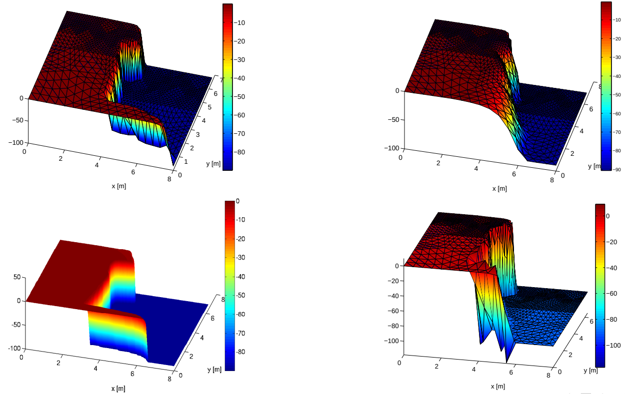

LN and SW performance

Method	Level	ε_{mc} at $T = 30[d]$	Avg. its.	Avg. CPU† [s]
CG-V-LN	3	1.18×10^{-7}	-	1.52×10^{-3} (5.62×10^{-3})
CG-V-SW	3	9.97×10^{-7}	451	3.13×10^{-1}
CG-S-LN	3	3.61×10^{-7}	-	1.52×10^{-3} (5.62×10^{-3})
CG-S-SW	3	1.00×10^{-6}	2289	1.58×10^{0}
CG-V-LN	4	2.09×10^{-7}	-	9.70×10^{-3} (2.49×10^{-2})
CG-V-SW	4	9.99×10^{-7}	377	9.74×10^{-1}
CG-S-LN	4	4.73×10^{-8}	-	9.70×10^{-3} (2.49×10^{-2})
CG-S-SW	4	1.00×10^{-6}	2072	5.39
CG-V-LN	5	5.37×10^{-7}	-	4.17×10^{-2} (1.14×10^{-1})
CG-V-SW	5	9.97×10^{-7}	185	2.13×10^{0}
CG-S-LN	5	1.52×10^{-7}	-	4.17×10^{-2} (1.14×10^{-1})
CG-S-SW	5	1.00×10^{-6}	584	8.20×10^{0}

† CPU required to build and factor LN node-star systems in parentheses

Revisiting P^1 nonconforming behavior for sharp fronts

At least two options to improve NC. Subgrid viscosity stabilization Alaoui and Ern (2006), and/or local refinement

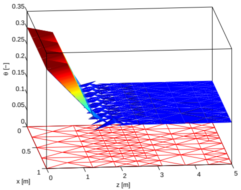

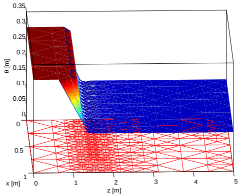

- Stabilization improved resolution of fronts but affected the distribution of velocity fields, particularly on very coarse grids.
- The velocity postprocessing approaches improved standard and stabilized CG approximations, and the combined CG strategies were competitive with mixed methods.
- The LN postprocessing was generally faster and more robust than the SW version. SW requires less storage and can be applied for generic velocity data.
- Velocity postprocessing algorithms are straightforward, inexpensive, and generally applicable. Better stabilization is needed, though.